ACS APPLIED MATERIALS & INTERFACES

Research Article

www.acsami.org

Boron Nitride Nanoparticles with a Petal-Like Surface as Anticancer Drug-Delivery Systems

Irina V. Sukhorukova,*[,†,§] Irina Y. Zhitnyak,[‡,§] Andrey M. Kovalskii,[†] Andrei T. Matveev,[†] Oleg I. Lebedev,[⊥] Xia Li,[∥] Natalia A. Gloushankova,[‡] Dmitri Golberg,*[,∥] and Dmitry V. Shtansky*[,†]

[†]National University of Science and Technology "MISIS", Leninsky prospect 4, Moscow 119049, Russia

[‡]N. N. Blokhin Russian Cancer Research Center, Kashirskoe shosse 24, Moscow 115478, Russia

[⊥]CRISMAT, UMR 6508, CNRS-ENSICAEN, 6Bd Marechal Juin, 14050 Caen, France

[∥]National Institute for Materials Science (NIMS), Namiki 1-1, Tsukuba, Ibaraki 3050044, Japan

ABSTRACT: Nanoparticles (NPs) have a great potential as nanosized drug-delivery carriers. Such systems must safely deliver the drug to the site of the tumor without drug leakage, effectively penetrate inside cancer cells, and provide intracellular drug release. Herein we developed an original and simple method aimed at the fabrication of spherical boron nitride NPs (BNNPs), 100−200 nm in diameter, with peculiar petal-like surfaces via chemical vapor deposition. Such structures were found to be able to absorb a large amount of antitumor drug-killing tumor cells. They revealed low cytotoxicity and rapid cellular uptake. BNNPs were saturated with doxorubicin (DOX) and then dispersed. The BNNPs loaded with DOX (BNNPs-DOX) were stable at neutral pH but effectively released DOX at pH 4.5−5.5. MTT assay and cell growth testing showed that the BNNPs-DOX nanocarriers had been toxic for IAR-6-1 cells. BNNPs loaded with DOX penetrated into the neoplastic IAR-6-1 cells using endocytic pathways, and then DOX released into the cytoplasm and cell nuclei and resulted in cell death.

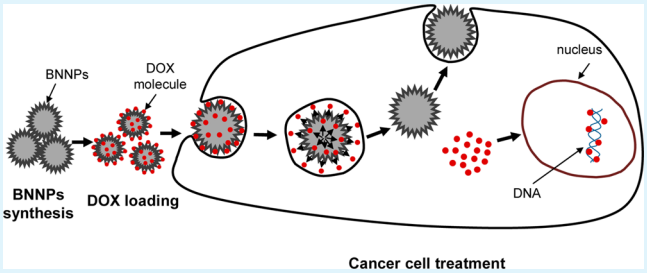

KEYWORDS: *BN nanoparticles, chemical vapor deposition, neoplastic cells, drug-delivery nanocarriers, doxorubicin, drug release*

1. INTRODUCTION

Despite considerable progress in the treatment of different forms of cancer, cell resistance to chemotherapeutic agents is still a challenge that the medical community has faced for many years, but decent materials have not been developed yet. Utilization of different types of nanoparticles (NPs), such as liposomes, polymer−drug conjugates, micelles, nanoshells, dendrimers, hydroxyl apatite, calcium phosphate, and metallic (gold, cadmium, and iron), porous ceramic (Fe_2O_3, SiO_2, TiO_2, Al_2O_3), and polymer NPs with sizes in the range of 10−500 nm, allows one to overcome some traditional therapeutic method limitations such as chemotherapy and/or radiotherapy.[1,2] The creation of a NP drug-delivery system is one of the promising methods that may solve the main chemotherapeutic problem known as multidrug resistance (MDR), which is mainly due to the overexpression of membrane-bound proteins that efflux drug from the cells.[3,4] Such anticancer drug-delivery nanocarriers must safely deliver the drug to the site of injury without drug leakage, effectively penetrate cancer cells using endocytosis mechanisms for nanocarrier uptake, and provide intracellular drug release to achieve an enhanced intracellular concentration that would cause the cells' death. For example, different types of metallic and polymer NPs loaded with doxorubicin (DOX) were shown to be effective in overcoming MDR in cancer therapy.[5−9] In the case of a drug-resistant form of neoplasia, in contrast to the drug alone, the therapeutic efficacy of DOX-loaded NPs was found to be higher[9−11] because of the higher accumulation of DOX in cancer cells.[9] Another advantage of the drug-delivery approach (based on the application of nanocarriers) is that it avoids the toxicity problems caused by a cytostatic and/or cytotoxic drug.[8,12]

The size and shape are critical parameters for drug-delivery particles. As far as the size of NPs is concerned, there are several factors that should be taken into account: the size of the smallest blood capillaries for the NPs that will be circulated in the blood vessels, the critical size to suppress NP removal via the reticuloendothelial system, the maximum size to allow NPs to easily penetrate into the diseased tissue, and the size that allows the NPs to diffuse through the entire tumor volume.[2] It is generally considered that the optimum particle size for drug-delivery carriers that ensures vascular permeability and maximizes drug accumulation in tumors is 100−150 nm.[2,13] NPs larger than 200 nm are sequestered in the liver, spleen, and kidneys, while those smaller than 100 nm may leave the blood vessels through fenestrations in the endothelial lining.[14]

Received: May 12, 2015
Accepted: July 20, 2015
Published: July 20, 2015

DOI: 10.1021/acsami.5b04101
ACS Appl. Mater. Interfaces 2015, 7, 17217−17225

Internalization of NPs by macrophages, which typically occurs for NPs larger than 500 nm, prevents the delivery of drugs to tumor cells.[15,16] Note that Qi et al.[17] reported an enhanced penetration and retention effect in tumor cells for somewhat smaller NPs, in the range of 50−100 nm. It was also reported that both uptake and removal of NPs were highly dependent upon the size and shape of the NPs.[18] Small NPs (~50 nm) were documented to be taken up faster and at higher concentration than other tested NPs.[19] Rod-shaped NPs showed a lower uptake in comparison to spherical-shaped NPs.[18]

Recent studies have revealed that multiwalled BN nanotubes (BNNTs) are not toxic. This opens up a broad prospective for their utilization as anticancer drug-delivery systems.[20,21] Note, however, that Horvàth et al.[22] reported a relevant toxicity of BNNTs, but additional experiments with the same but shortened (a length of 1.5 μm versus the former 10 μm) multiwalled BNNTs demonstrated no toxic effects.[23] These results indicate that the size and shape of BNNTs play a critical role in material cytocompatibility. Multiwalled BNNTs functionalized with mesoporous silica and multimodal luminescent−magnetic BNNTs@NaGdF4:Eu structures for cancer therapy were also reported.[24,25]

The spherical shape of a drug carrier is of special interest because of a large contact area with cell membrane receptors. The present paper is focused on the fabrication of BNNPs with a petal-like surface structure, which are able to absorb a large amount of antitumor drug, and their utilization by neoplastic cells.

2. MATERIALS AND METHODS

2.1. Synthesis and Dispersion of BNNPs. BNNPs with an average external diameter of 100−200 nm were prepared by chemical vapor deposition (CVD) using boron oxide vapor and flowing ammonia in a vertical induction furnace (Figure 1). The temperature in the precursor location area was maintained at 1310 °C. The powder mixture of pure FeO, analytical-grade MgO, and B (>99%) taken at a weight ratio of 150:28:75 was used as a precursor. The powders were mechanically ground in an alumina mortar for 1 h. After homogenization, the BN ceramic crucible filled with the precursor was put into a BN reactor and placed in a heating zone. Another BN ceramic crucible for the collection of BNNPs during the synthesis was placed in front of the hole drilled in the upper part of the reactor wall outside of the heating zone (Figure 1).

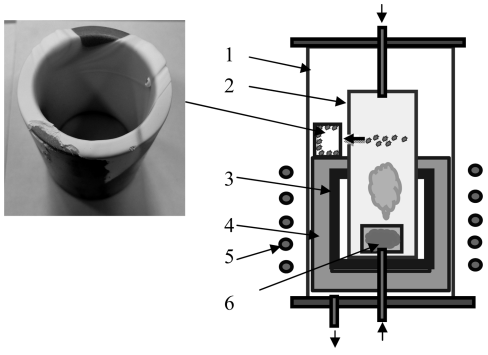

Figure 1. BN crucible with synthesized products seen as a white-color film (left) and a scheme of the CVD process: 1, SiO_2 furnace chamber; 2, BN reactor; 3, carbon susceptor (heating element); 4, carbon lining; 5, inductor; 6, BN crucible with a precursor. Gas flows: NH_3 (from the top) and Ar (from the bottom).

Boron oxide vapor as a source of boron for the CVD reaction with ammonia gas (99.98%) was generated during the following oxidation reactions within the precursor:[26]

$$2B(s) + 2MgO(s) \rightarrow B_2O_2(g) + 2Mg(g) \quad (1)$$

$$2B(s) + 2FeO(s) \rightarrow B_2O_2(g) + 2Fe(g) \quad (2)$$

BNNPs were synthesized using the following reaction of boron oxide vapor with ammonia:

$$B_2O_2(g) + 2NH_3(g) \rightarrow 2BN(s) + 2H_2O(g) + H_2(g) \quad (3)$$

Boron oxide vapor was transported to the reaction zone with ammonia by an argon flow. During the synthesis, the Ar/NH_3 flow ratio was maintained at 2. To reduce the oxygen impurities in the synthetic products, the oxygen getter was used (pieces of iron foil and titanium bar were placed in the heating zone).

The reaction of boron oxide vapor with ammonia took place in the upper part of the reactor in the temperature gradient zone; therefore, the CVD process of BNNPs was realized at somewhat lower temperatures. The synthesis was carried out for 200 min. During the synthesis, a flow of the white smog coming out of the hole in the reactor wall (toward the small BN crucible) was continuously observed. After the synthesis, a white color film was found to entirely cover the BN crucible walls (Figure 1). Typically, using 10 g of the precursor was enough to synthesize about 250−400 mg of BNNPs in 6 h.

After the synthesis, the BNNPs were agglomerated. In order to separate the agglomerates into individual NPs, BNNPs were ultrasonically treated in a distilled water solution (BNNP concentration 2 mg/mL) using a Bandelin Sonoplus HD2200 unit (Germany) at a power of 80 W for 30 min.

2.2. Characterization of BNNPs. The morphology of synthesized products and their chemical compositions were studied using a JEOL JSM-7600F scanning electron microscope equipped with an energy-dispersive X-ray (EDX) detector. Transmission electron microscopy (TEM), including high-resolution (HRTEM) imaging and selected-area electron diffraction (SAED), was carried out using a Tecnai G2 30 UT microscope operated at 300 kV and having 0.17 nm spatial resolution. Chemical and phase compositions were analyzed by EDX spectroscopy (using an 80 mm^2 X-Max EDX detector, Oxford Instruments), X-ray diffraction (XRD) analysis [using a Difrei-401 X-ray diffractometer equipped with a coordinated charge-coupled detector and operating with Cr Kα radiation], and Fourier transform infrared spectroscopy (FTIR; with a Bruker Vertex 70v vacuum spectrometer) in the range of 400−2000 cm^{-1} using a partial internal reflection device. The particle size distribution was estimated using a dynamic light scattering method on a particle size analyzer (Zetasizer Nano ZS). For each sample, three measurements were made. To control the size of the particles and agglomerates, 1 μL of the suspension was dropped onto a silicon substrate for scanning electron microscopy (SEM) analysis.

2.3. Stability of BNNPs in Earle's Balanced Salt Solution (EBBS). BNNPs (2 mg/mL) were soaked in 40 mL of EBBS for 14 days. After the tests, the BNNPs were rinsed in distilled water three times and then centrifuged. The particle size and morphology before and after the tests were controlled by SEM.

2.4. Saturation of BNNPs with DOX. BNNPs (2 mg) were added to 1 mL of 0.5, 1.0, or 2.5 mg/mL DOX solutions. The suspensions were incubated at room temperature for 24 h. The precipitates were then washed out from the DOX in water 10 times under repeated centrifugation at 13400 rpm for 15 min.

2.5. Drug Release. For the drug-release study, 4 mg of BNNPs-DOX was suspended in either 5 mL of phosphate buffer saline (PBS) or 0.1 M sodium acetate buffer (NaAc) at different pH values (pH 4.4, 5.4, and 7.4). The samples were incubated at 37 °C for various periods of time. At different time points (0.25, 1, 2, 4, 6, 8, 24, and 48 h), supernatant samples (0.2 mL) were analyzed by UV−visible spectroscopy using a ND-3300 fluorospectrometer (Thermo Scientific, USA) under the following conditions: excitation at 470 nm and emission at 596 nm.

DOI: 10.1021/acsami.5b04101
ACS Appl. Mater. Interfaces 2015, 7, 17217−17225

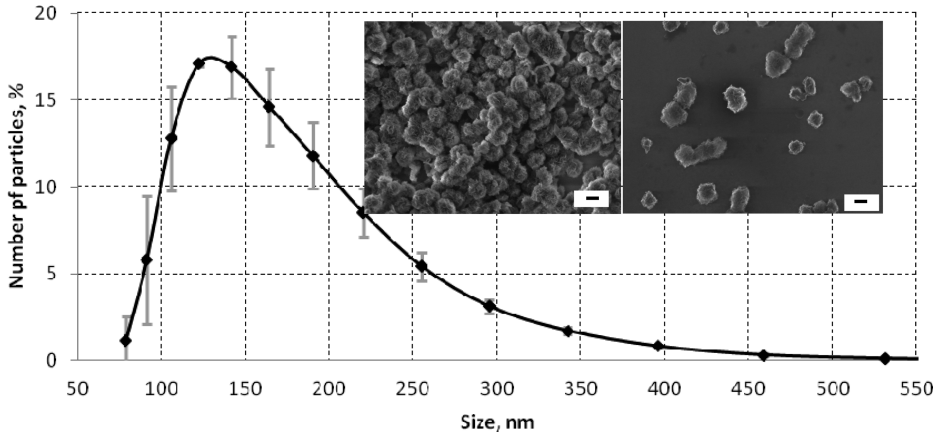

Figure 2. Particle size distribution after ultrasonic treatment. The insets show the size of the BNNPs before (left) and after (right) ultrasonic treatment. The scale bars on the insets correspond to 100 nm.

2.6. Cell Culture. The IAR-6-1 line of neoplastically transformed with dimethylnitrosamine epithelial cells was obtained from Dr. Montesano (International Agency for Research of Cancer, Lyon, France). The cells were tumorigenic in nude mice. The cells were cultured in Dulbecco's modified Eagle's medium (DMEM; Sigma, USA) supplemented with 7.5% fetal bovine serum (FBS; PAA Laboratories, Austria), penicillin (100 IU/mL), and streptomycin (100 μg/mL) at 37 °C in a 5% CO_2-humidified atmosphere.

2.7. MTT Assay. IAR-6-1 cells were seeded into 96-well plates (2×10^4 cells/mL) with DMEM supplemented with 7.5% FBS, penicillin, and streptomycin. After 24 h, the prescribed amounts of BNNPs, BNNPs-DOX, or free DOX at different concentrations were added to the medium, and the cells were incubated for 72 h. For saturation of BNNPs with a DOX solution, a 0.5 mg/mL DOX solution was used. The culture medium was carefully selected and replaced by a fresh FBS-free medium. A total of 20 μL of MTT reagent [3-(4,5-dimethylthiazol-2-yl)-2,5-diphenyl-2*H*-tetrazolium bromide, 5 mg/mL, Sigma, USA] was added to each well. After incubation for 4 h, the supernatant was carefully aspirated, and MTT formazan generated by live cells was dissolved in 150 μL of dimethyl sulfoxide (DMSO) for 20 min. The absorbance at a wavelength of 570 nm was measured using a Benchmark Plus microplate spectrophotometer (Bio-Rad, USA). Nontreated cells were used as a control. The absorbance was normalized to the blank (150 μL of DMSO) and expressed as a percent of viable cells.

2.8. Proliferation of IAR-6-1 Cells. IAR-6-1 cells were seeded into a 24-well plates. After 24 h, either BNNPs or BNNPs-DOX at different concentrations were added to the medium. For saturation of BNNPs with a DOX solution, a 0.5 mg/mL DOX solution was used. Equivalent concentrations of free DOX were also used. Pure water (13 μL) was used as a control. At 24, 48, and 72 h after the beginning of incubation, the cells were fixed with 3.7% paraformaldehyde (PFA) for 10 min and then stained with 4′,6-diamidino-2-phenylindole (DAPI) for 40 min. The nuclei stained with DAPI were counted in 30 fields using a Zeiss Axioplan fluorescent microscope.

2.9. Cellular Uptake of BNNPs-DOX. IAR-6-1 cells were seeded into 60 mm culture dishes and incubated for 24 h. Cells were preincubated with dynasore (100 μM) for 30 min. Thereafter, cells were incubated with BNNPs-DOX (the final concentration of BNNPs was 100 μg/mL) at 37 °C for 24 h in the presence of an inhibitor. Control cells were incubated with BNNPs-DOX without an inhibitor. Cells were thoroughly washed and lysed with Mg^{2+} Lysis/Wash Buffer (Upstate EMD Millipore). In supernatant samples, DOX-related fluorescence was measured by UV−visible spectroscopy using a ND-3300 fluorospectrometer at excitation and emission wavelengths of 470 and 596 nm, respectively.

2.10. Internalization of BNNPs by Cells and Fluorescence Imaging. IAR-6-1 cells were seeded into 35 mm glass bottom culture dishes (MatTeck Corp, USA) and incubated for 24 h. A total of 0.2 mL of a BNNPs-DOX suspension was added to the cell culture in FBS-free media (the final concentration of BNNPs was 100 μg/mL). After 7 h of incubation with BNNPs, the cells were fixed with 3.7% PFA for 10 min, permeabilized with 0.5% Triton X-100 (Sigma, USA) for 5 min, and stained with Alexa488-phalloidin (Molecular Probes, Life Technologies, USA) for 40 min to visualize the actin cytoskeleton. The mounted samples were examined with a Leica TCS SP5 confocal laser scanning microscope equipped with an HDX PL APO 100× 1.4 objective. For staining with LysoTracker, IAR-6-1 cells were incubated with BNNPs-DOX for 4 h and then incubated with LysoTracker Green DND-26 (50 nM) for 30 min at 37 °C. The cells were washed four times with a fresh medium and examined by confocal laser scanning microscopy (CLSM).

3. RESULTS

3.1. Size of BNNPs. The results of particle size analysis after ultrasonic treatment are presented in Figure 2. It can be seen that a major fraction of BNNPs (about 80%) falls within the range of 100−200 nm. As revealed by SEM observations (Figure 2, inset) and also confirmed by TEM, the BNNPs were perfectly separated from each other.

3.2. Structure of BNNPs. As follows from SEM analysis, the synthesized product consists of agglomerates of spherical BNNPs with an average size of 100−200 nm (Figure 3a,b). Their surface is formed by numerous nanosheet-like petals. The magnified SEM image reveals that the pompon-like nanospheres are composed of layered nanoflakes with a thickness of about 3−5 nm protruding outward from the center (Figure 3c). Note that in the synthesized products a minor fraction of hollow spherical BNNPs with a smooth surface was also observed. EDX analysis revealed the presence of boron, nitrogen, and oxygen species, and the B/N ratio was close to 1. The oxygen content in the agglomerates was about 2−10 atom %. The formation of BNNPs with a hexagonal structure was additionally confirmed by XRD (not shown) and FTIR spectroscopy (the results are presented below).

Figure 4a shows the bright-field (BF) low-magnification TEM image of BNNPs. The synthesized products consist of round-shaped NPs with an average size of 100−200 nm. The corresponding SAED pattern taken from the number of BNNPs exhibits two diffuse rings with d spacings roughly corresponding to the typical hexagonal BN interplanar spacings (d_{002} and d_{100}). EDX analysis of single BNNPs confirmed the SEM results and revealed the presence of boron and nitrogen species demonstrating the high purity of BNNPs. TEM analysis performed at higher magnification clearly showed that BNNPs have a hollow spherical central part and multiple petals made of

DOI: 10.1021/acsami.5b04101
ACS Appl. Mater. Interfaces 2015, 7, 17217−17225

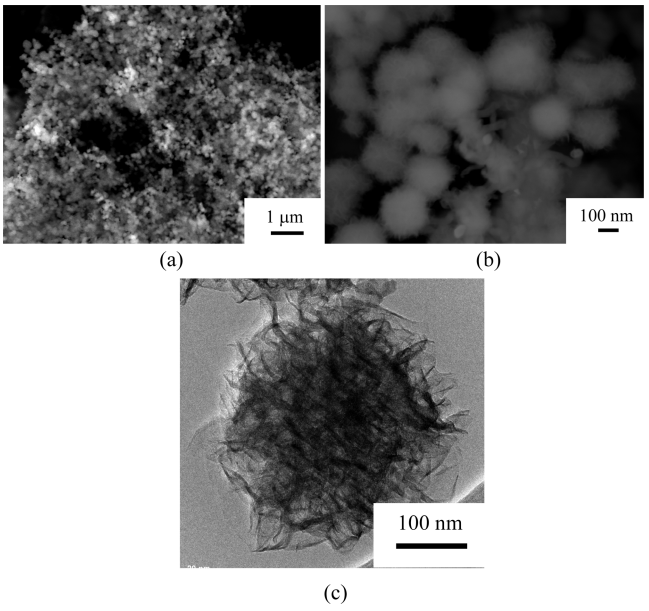

Figure 3. (a and b) SEM images at various magnifications of agglomerates of BNNPs with an average size of 100−200 nm obtained at T = 1310 °C. (c) TEM image of a single BNNP with petal-like surface structure.

exposed BN layers at the side area (Figure 4b). Our TEM results clearly indicated that BNNPs had a porous-like morphology somewhat similar to that reported by Terrones et al.[27] but certainly different due to the presence of a hollow space in their cores. The HRTEM image of the near surface area is shown in Figure 4c. The surface of the BNNPs is formed by erecting BN layers consisting of 2−6 BN stacked atomic layers. The HRTEM image (Figure 4c, inset) also suggests that the layers are not open and highly curled, covering the inner spherical part. Such BNNPs with petal-like surface structure appear to be suitable for effective anticancer drug loading and their transfer to cancer cells.

The as-received BNNPs were additionally characterized using FTIR spectroscopy. Figure 5 compares the IR spectra of BNNPs and a commercial BN powder. The BN powder is characterized by two features in the FTIR spectrum: a sharp low-wavenumber mode at 769 cm^{-1} and a broad high-wavenumber mode at 1359 cm^{-1}, which correspond to out-of-plane B−N−B bending and in-plane B−N stretching vibrations, respectively.[28] These peaks are the fingerprints of sp^2-bonded BN. The FTIR spectrum from BNNPs had two additional features: a small peak at 910 cm^{-1} and a region with high absorbance between 400 and 720 cm^{-1}. These two additional features can be taken as an indication of the presence of some amount of oxygen impurities.[28,29]

3.3. Stability of BNNPs in EBBS. The stability of BNNPs was studied during their incubation in EBBS for 14 days (Figure 6). It can be seen that chemical treatment in EBBS did not affect the average size and morphology of BNNPs. The petal-like surface was also preserved.

3.4. Drug Loading Capacity of BNNPs. The DOX content in the BNNPs was determined using two different approaches, and the results were similar. In the first method, the amount of DOX loaded into BNNPs was detected by comparing the intensities of the UV−visible absorption of DOX at 480 nm for the initial DOX solution used for loading of BNNPs and for that of the supernatant DOX solution after

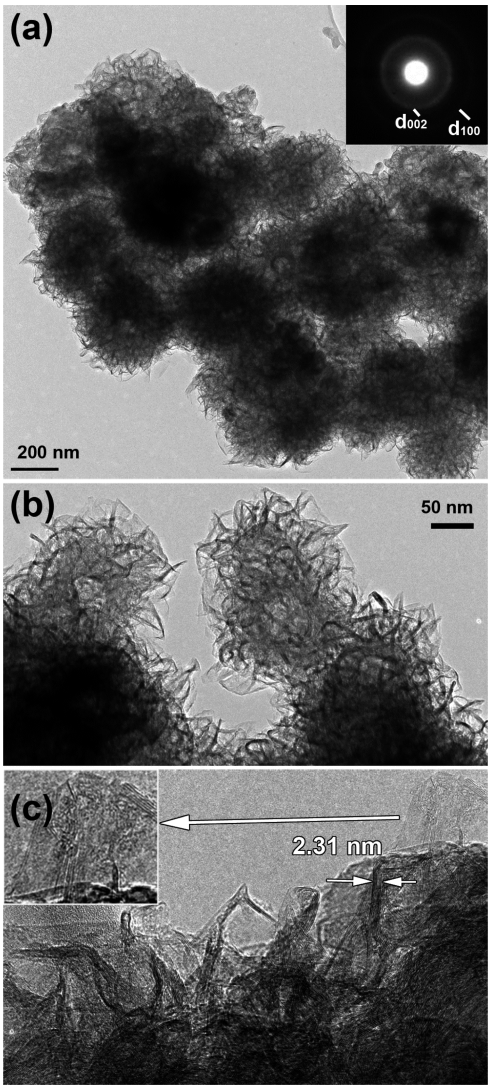

Figure 4. (a) BF low-magnification TEM image of a BNNPs agglomerate and corresponding SAED pattern (inset). (b) Enlarged image of BNNPs. (c) HRTEM image of the side region of BNNPs. A close-up image of the surface of BNNPs consisting of spiky-type BN layers is given in the inset.

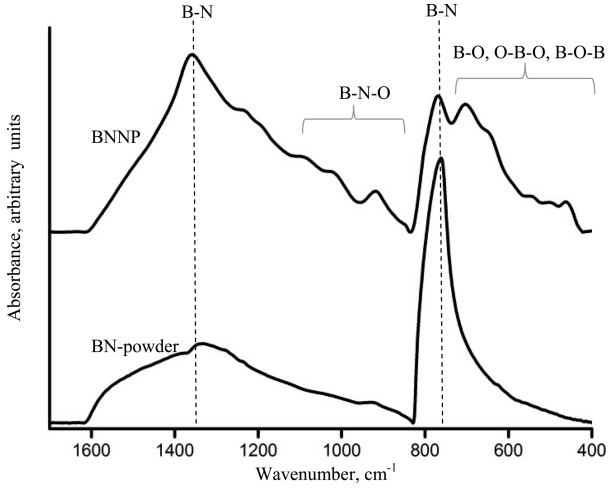

Figure 5. Comparative FTIR spectra of BNNPs and a commercial BN powder.

DOI: 10.1021/acsami.5b04101
ACS Appl. Mater. Interfaces 2015, 7, 17217−17225

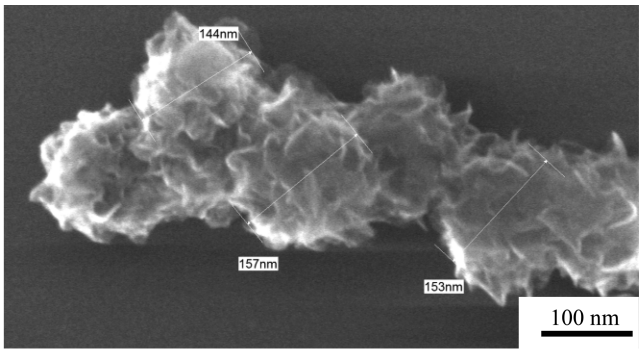

(a)

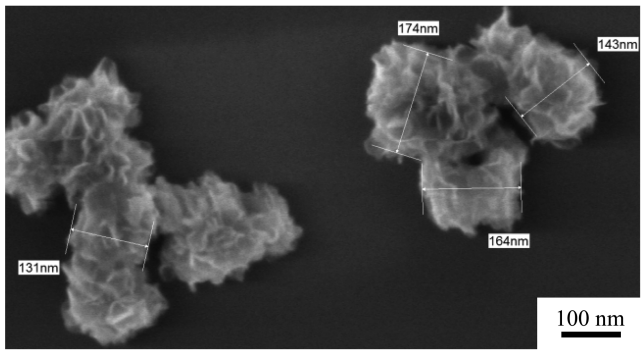

(b)

Figure 6. SEM images of BNNPs (a) before and (b) after soaking in EBBS for 14 days.

removal of all BNNPs-DOX. In the second method, the DOX content in BNNPs-DOX was determined after dissolving BNNPs-DOX in DMSO for 20 h and by measuring the fluorescence of supernatants at excitation and emission wavelengths of 485 and 590 nm, respectively. The highest DOX loading capacity of BNNPs was documented to be 0.055 mg/mg of NPs.

3.5. pH-Dependent Drug Release. BNNPs-DOX nanocarriers were incubated in PBS or acetate buffers at different pH values after the fluorescence emission spectra in the supernatant were measured at different time intervals. As shown in Figure 7, incubation of BNNPs-DOX in PBS and acetate buffer at pH 4.4 and 5.4 led to a rapid recovery of fluorescence (the results are presented as the dependence of relative fluorescence units (RFU) versus time). Incubation of BNNPs-DOX in PBS

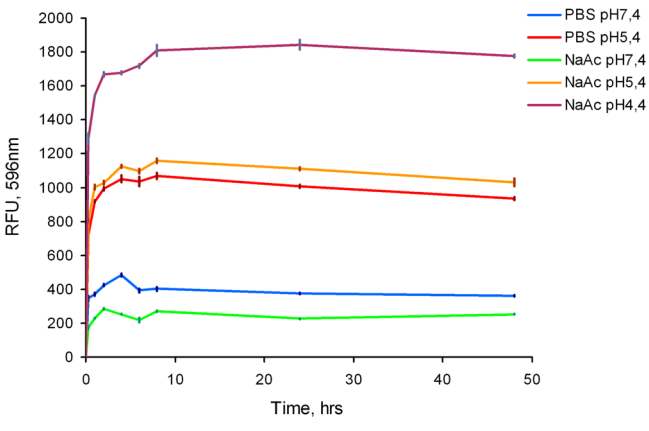

Figure 7. pH-dependent DOX release from BNNPs-DOX versus time.

at pH 7.4 did not lead to significant fluorescence recovery after 50 h of incubation. These data demonstrate that BNNPs-DOX are relatively stable at neutral pH, whereas DOX is effectively released from the BNNPs at acidic pH (pH 4.5−5.5) under conditions comparable to those found in endosomes/lysosomes. As a control, the fluorescence intensity of free DOX was measured in buffers with pH 4.4, 5.4, and 7.4 (Table 1).

Table 1. Fluorescence Intensity of Free DOX at Different pH Values

	RFU		
DOX concentration, μg/mL	pH 7.4	pH 5.4	pH 4.4
5	1068 ± 20	1435 ± 25	1649 ± 28
2.5	493 ± 10	776 ± 12	889 ± 18
1	151 ± 7	287 ± 5	365 ± 8

3.6. Cytotoxicity of BNNPs-DOX Nanocarriers. The cytotoxic effect of BNNPs-DOX cells was evaluated by MTT assay in IAR-6-1 cells (Figure 8). The cytotoxicity of free DOX was compared to that of BNNPs-DOX at equivalent DOX doses and nondrug-loaded BNNPs. The DOX-loaded NPs were found to be toxic to IAR-6-1 cells. The cytotoxicity of BNNPs-DOX was comparable with free DOX at identical concentrations, in the range 0.26−1.04 μg/mL. Note that at high BNNP concentration the viability of the cells slightly decreased. Thus, the present results support the conclusion of Ciofani et al.,[30] who suggested that the decrease in the cell viability at high BNNT concentration (>20 μg/mL) can be wrongly interpreted as the cytotoxicity due to BN nanophase interaction with some tetrazolium salts. A similar effect was also reported for carbon NTs.[31]

We also investigated the growth of IAR-6-1 cells in the presence of BNNPs, BNNPs-DOX, and free DOX (control). The alterations in the cell density for 72 h are shown in Figure 9. In the presence of either DOX or BNNPs-DOX, the proliferation of the cells was markedly decreased. BNNPs themselves (in a concentration up to 40 μg/mL) did not affect the growth of IAR-6-1 neoplastic cells. We did not see any statistically significant differences in a number of cells cultivated in the presence of BNNPs and pure water.

3.7. Uptake of BNNPs-DOX by Neoplastic Cells. Using CLSM, cellular uptake of BNNPs loaded with DOX by IAR-6-1 neoplastic cells was studied. After 7 h of incubation with BNNPs loaded with DOX, IAR-6-1 cells were fixed and stained with Alexa488-phalloidin to visualize the main cytoplasmic system, actin cytoskeleton. As shown in Figure 10, BNNPs-DOX were internalized by IAR-6-1 neoplastic cells and distributed in cell cytoplasm near the nucleus. Red fluorescence of DOX inside the nucleus was also clearly visible. As revealed at XZY optical slices, BNNPs-DOX are absorbed by cells and seen in cell cytoplasm between actin, showing perinuclear enrichment. To confirm the endosomal-mediated uptake of BNNPs-DOX, LysoTracker Green, which labels highly acidic compartments within live cells, was used. We compared the intracellular localization of BNNPs-DOX and of endosomal/lysosomal compartments. CLSM showed that most of the BNNPs-DOX had been colocalized with LysoTracker, indicating that BNNPs-DOX are located in the endosomes/lysosomes after 4 h of uptake (Figure 11a). We have also studied the effect of dynasore, an inhibitor of dynamin GTPase activity, which blocks dynamin-dependent endocytosis in

DOI: 10.1021/acsami.5b04101
ACS Appl. Mater. Interfaces 2015, 7, 17217−17225

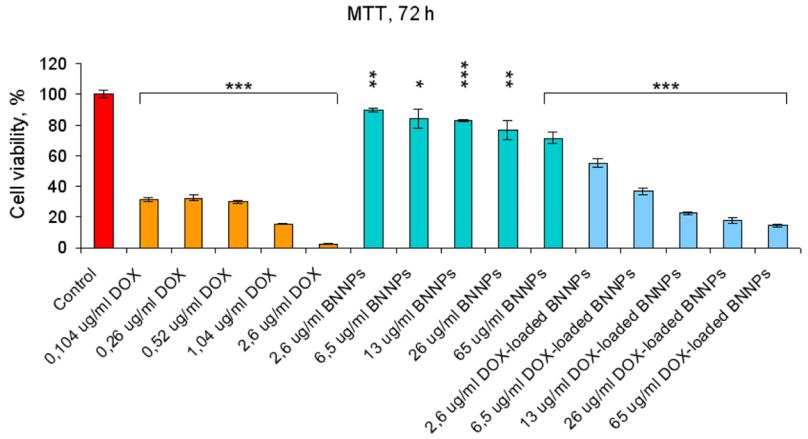

Figure 8. Effects of DOX, pristine BNNPs, and DOX-loaded BNNPs on the cell viability. DOX content = 0.04 mg/mg of particles. MTT assay (*, $p < 0.05$; **, $p < 0.005$; ***, $p < 0.001$) indicates statistically significant differences in comparison with the control (Kruskal–Wallis test).

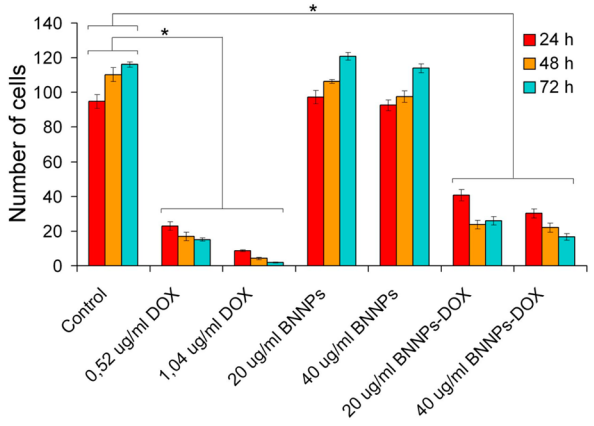

Figure 9. Cell density in cultures of IAR-6-1 cells growing for 72 h in the presence of BNNPs, BNNPs-DOX, and free DOX. DOX content = 0.026 mg/mg of particles. A value of $p < 0.001$ indicates statistically significant differences in comparison with the control (Kruskal–Wallis test).

cells.[32] As shown in Figure 11b, treatment of the culture with dynasore reduced the accumulation of DOX in IAR-6-1 cells incubated with BNNPs-DOX for 24 h. Dynasore-treated cells showed a weaker DOX-related fluorescent intensity than control cells.

Using CLSM, we also imaged neoplastic IAR-6-1 cells after 5 days of incubation with BNNPs-DOX. DOX was observed to be distributed in both cytoplasma and nuclei of IAR-6-1 cells (Figure 12). It can be seen that DOX accumulation in the cells resulted in typical changes associated with cell death, as was evident by the condensation and fragmentation of the nuclei. These experiments showed that BNNPs-DOX internalized into IAR-6-1 neoplastic cells, with DOX released from BNNPs, had accumulated in both cytoplasma and nuclei and promoted cell death.

4. DISCUSSION

Most chemotherapeutic drugs can pass through the cell membrane of tumor cells via diffusion. However, in the course of treatment, many cancers acquire resistance to the chemotherapeutic drug, which is often due to the overexpression of ATP-binding cassette transporters (ABC transporters) that efflux drug from the cells.[33] Using nanosized drug-delivery systems allows one to overcome the mechanisms of MDR of cancers and to enhance therapeutic efficacies of drugs.[34] Here we report that BNNPs are capable of loading and delivering the chemotherapeutic drug (DOX) inside neoplastic cells.

We found that BNNPs had low cytotoxicity, high drug loading efficacy (0.055 mg/mg of BNNPs-DOX), and rapid cellular uptake. The ways of entering of DOX-loaded BNNPs into cells are not known exactly. Possibly, caveolin- or clathrin-mediated endocytosis plays a role in their cell uptake. Using LysoTracker Green, we showed that BNNPs had been accumulated in endosomal/lysosomal compartments. Acidification of endosomes may contribute to the drug release. This question obviously needs further investigation with the usage of specific inhibitors of various endocytic pathways.

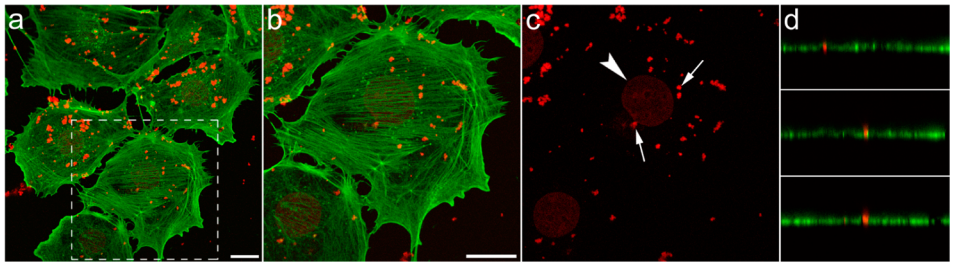

Figure 10. CLSM images of BNNPs-DOX in IAR-6-1 neoplastic cells after 7 h of incubation. (b and c) Close-up views of the boxed region from part a. (a and b) Alexa488-phalloidin staining of actin cytoskeleton (green) and fluorescence of DOX (red), (c) fluorescence of DOX, (d) z slides of the cell. BNNPs-DOX are seen near the nucleus (arrows). Note the red fluorescence of DOX in the nucleus (arrowhead). Final concentration of BNNPs-DOX in media = 100 μg/mL. Scale bar = 10 μm.

DOI: 10.1021/acsami.5b04101
ACS Appl. Mater. Interfaces 2015, 7, 17217–17225

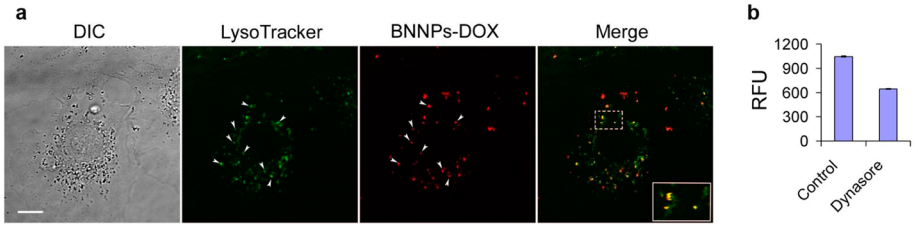

Figure 11. (a) CLSM images of IAR-6-1 cells incubated with BNNPs-DOX for 4 h. Cells were stained with LysoTracker Green. BNNPs-DOX (red) are colocalized with LysoTracker Green (arrowheads). In the boxed region, the zones of colocalization of BNNPs-DOX and LysoTracker Green appear yellow. (b) Effect of dynasore on the DOX-related fluorescent intensity in the cells incubated with BNNPs-DOX for 24 h.

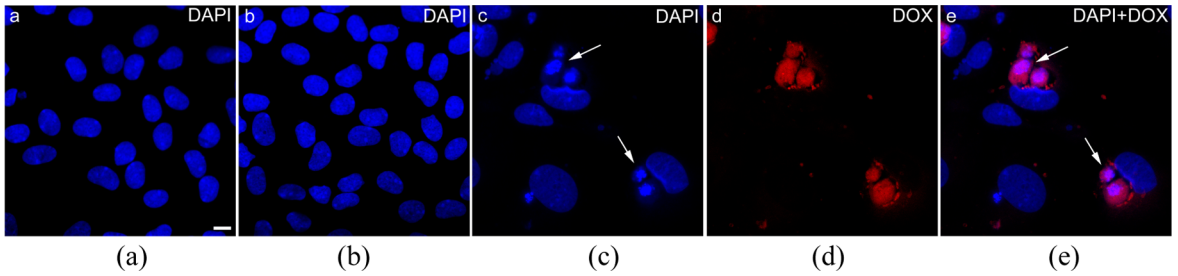

Figure 12. CLSM images of IAR-6-1 cells stained with DAPI: (a) control culture; (b) cells cultivated in the presence of BNNPs (13 μg/mL) for 5 days. Cells cultivated in the presence of BNNPs-DOX for 5 days: (c) DAPI fluorescence of nuclei; (d) DOX fluorescence in cells; (e) overlay of blue and red channels. Chromatin condensation and fragmentation of nuclei are shown by arrows. Scale bar = 10 μm.

BNNPs have a great potential for use as nanosized drug-delivery carriers, for example, for treatment of ovarian carcinomas that grow rapidly and metastasize early. Unlike most other cancers, ovarian carcinoma rarely disseminates through vasculature. These types of carcinomas metastasize within the peritoneal cavity.[35] Cancer cell spheroids are carried by the physiological movement of peritoneal fluid and attach preferentially to the abdominal peritoneum or omentum, where they only invade the superficial bowel serosa and never the deeper layers. In the case of metastatic ovarian carcinoma, intraperitoneal delivery of the chemotherapeutic drugs increases survival compared with intravenosus administration. Nanosized BNNPs loaded with a drug can be utilized for the treatment of ovarian cancers resistant to chemotherapeutic drugs.

Usually, drug release from the surface of smooth particles occurs within a few hours.[36,37] Approaches to overcome this problem include the fabrication of NPs with a rough surface or use of protective films to slow drug release. For instance, the duration of full DOX release from mesoporous silica NPs was reported to be 50[38] and 80 h for smaller particles (about 60 nm).[39] Poly(amidoamine) dendrimer-coated magnetic NPs were shown to keep DOX for more than 24 h.[40] A hydrogel system comprised of biocompatible aminated guar gum, Fe_3O_4–ZnS core–shell NPs, and DOX hydrochloride was able to provide a slow DOX release for 20 days.[41] Quantitative measurements of DOX fluorescence performed in the present study showed that BNNPs with a petal-like surface structure are capable of holding DOX for at least 7 days. The particle surface charge and acidity are other factors to be taken into consideration. The particle surface charge may affect the drug loading capacity because of electronic interaction between the NPs and DOX.[42] DOX release is strongly pH-dependent, and its intensive release is usually observed during exposure in an acidic environment.[42,43] Our data demonstrate that BNNPs-DOX nanocarriers are relatively stable at neutral pH, whereas DOX is effectively released at acidic pH (pH 4.5–5.5) under conditions comparable to that found in endosomes/lysosomes. A more detailed study of the influence of DOX-loaded BNNPs with a petal-like surface structure on the drug-resistant forms of neoplasia will be addressed in our future work.

Finally, it can be concluded that BNNPs are one of the most promising materials for cancer therapy because of the combination of their high chemical stability, uniformity, and dispersibility in a solution. Structural special features such as a hollow spherical central part and a highly developed outer surface with numerous petals make BNNPs ideal nanocarriers for the delivery of anticancer drug to target areas. The needlelike surface of BNNPs may be useful for their more effective penetration into the endosomes. Because of the lack of chemical bonding between the wide-band-gap BN and biological molecules (for instance, glycine)[44] and high binding energy between BN and physically adsorbed biological molecules (such as guanine and thiazole),[45,46] BN nanophases were shown to be suitable for the delivery of biological molecules to cancer cells. Future works can be focused on the additional functionalization of BNNPs to further improve their biological performance, similar to that of BNNTs. For instance, the surface of BNNTs was successfully functionalized by gold NPs, which are known to be the universal linker to biological molecules.[47] The strong links between BNNTs and human transferrin were demonstrated by Ciofanni et al.[48] It is known that transferrin is highly attracted to the cancer cells compared to healthy cells and therefore can provide the selectivity in cancer therapy. BNNTs were functionalized by folat groups, resulting in a significant increase in their uptake by cells.[49] Additional potential applications of BNNPs include their utilization for boron neutron capture therapy, where BNNPs could promote a high boron concentration,[50,51] or as bionanotransducers for cell sensing and stimulation because of their specific piezoelectric properties.[52−54]

DOI: 10.1021/acsami.5b04101
ACS Appl. Mater. Interfaces 2015, 7, 17217−17225

5. CONCLUSIONS

High-purity spherical BNNPs, 100−200 nm in diameter, with highly developed petal-like surfaces were fabricated by the CVD method using boron oxide vapor and flowing ammonia in a vertical induction furnace. Thorough structural characterization revealed that the surface of hollow BNNPs had been made of numerous nanosheet petals. Such BNNPs with ultimately porous structures can be utilized as nanocontainers for the delivery of various chemotherapeutic agents in chemotherapy-resistant tumor cells. The chemical treatment in EBBS for 14 days did not affect the average size and morphology of BNNPs. The BNNPs loaded with DOX were stable at neutral pH but effectively released DOX at pH 4.5−5.5. MTT assay and cell growth tests showed that BNNPs-DOX had been toxic for neoplastic IAR-6-1 cells. The cytotoxicity of BNNPs-DOX was comparable with that of free DOX at identical concentrations in the range of 0.26−1.04 μg/mL. The BNNPs-DOX nanocarriers were internalized into IAR-6-1 neoplastic cells using endocytic pathways, and then DOX was released from nanosized drug-delivery carriers and accumulated in both nuclei and cytoplasma, resulting in cell death.

AUTHOR INFORMATION

Corresponding Authors

*E-mail: irina_btnn@mail.ru.
*E-mail: golberg.dmitri@nims.go.jp.
*E-mail: shtansky@shs.misis.ru.

Author Contributions

§These authors contributed equally to this work.

Notes

The authors declare no competing financial interest.

ACKNOWLEDGMENTS

The work was supported by the Ministry of Education and Science of the Russian Federation (Increase Competitiveness Program of NUST "MISiS" Grant K2-2015-001 in the frame of "Mega-Grant" Award Grant 11.G34.31.0061 and State Task 11.1077.2014/K). O.I.L. is grateful for the financial support of the Ministry of Education and Science of the Russian Federation in the framework of Increase Competitiveness Program of the National University of Science and Technology "MISIS" (Grant K3-2014-021).

REFERENCES

(1) Zhang, L.; Gu, F. X.; Chan, J. M.; Wang, A. Z.; Langer, R. S.; Farokhzad, O. C. Nanoparticles in Medicine: Therapeutic Applications and Developments. *Clin. Pharmacol. Ther.* **2008**, *83*, 761−769.

(2) Fukumori, Y.; Ichikawa, H. Nanoparticles for Cancer Therapy and Diagnosis. *Adv. Powder Technol.* **2006**, *17*, 1−28.

(3) Kane, S. E. Multidrug Resistance of Cancer Cells. *Adv. Drug Res.* **1996**, *28*, 181−252.

(4) Bolhuis, H.; van Veen, H. W.; Poolman, B.; Driessen, A. J. M.; Konings, W. N. Mechanism of Multidrug Transporters. *FEMS Microbiol. Rev.* **1997**, *21*, 55−84.

(5) Soma, C. E.; Dubernet, C.; Barratt, G.; Nemati, F.; Appel, M.; Benita, S.; Couvreur, P. Ability of Doxorubicin-loaded Nanoparticles to Overcome Multidrug Resistance of Tumor Cells After Their Capture by Macrophages. *Pharm. Res.* **1999**, *16*, 1710−1716.

(6) Wang, F.; Wang, Y. C.; Dou, S.; Xiong, M. H.; Sun, T. M.; Wang, J. Doxorubicin-tethered Responsive Gold Nanoparticles Facilitate Intracellular Drug Delivery for Overcoming Multidrug Resistance in Cancer Cells. *ACS Nano* **2011**, *5*, 3679−3692.

(7) Kievit, F. M.; Wang, F. Y.; Fang, C.; Mok, H.; Wang, K.; Silber, J. R.; Ellenbogen, R. G.; Zhang, M. Doxorubicin Loaded Iron Oxide Nanoparticles Overcome Multidrug Resistance in Cancer in Vitro. *J. Controlled Release* **2011**, *152*, 76−83.

(8) Park, J.; Fong, P. M.; Lu, J.; Russell, K. S.; Booth, C. J.; Saltzman, W. M.; Fahmy, T. M. PEGylated PLGA Nanoparticles for the Improved Delivery of Doxorubicin. *Nanomedicine* **2009**, *5*, 410−418.

(9) Kang, K. W.; Chun, M. K.; Kim, O.; Subedi, R. K.; Ahn, S. G.; Yoon, J. H.; Choi, H. K. Doxorubicin-loaded Solid Lipid Nanoparticles to Overcome Multidrug Resistance in Cancer Therapy. *Nanomedicine* **2010**, *6*, 210−213.

(10) Soma, C. E.; Dubernet, C.; Barratt, G.; Benita, S.; Couvreur, P. Investigation of the Role of Macrophages on the Cytotoxicity of Doxorubicin and Doxorubicin-loaded Nanoparticles on M5076 Cells in Vitro. *J. Controlled Release* **2000**, *68*, 283−289.

(11) Chiannilkulchai, N.; Driouich, Z.; Benoit, J. P.; Parodi, A. L.; Couvreur, P. Doxorubicin-loaded Nanoparticles: Increased Efficiency in Murine Hepatic Metastases. *Sel. Cancer Ther.* **1989**, *5*, 1−11.

(12) Steiniger, S. C. J.; Kreuter, J.; Khalansky, A. S.; Skidan, I. N.; Bobruskin, A. I.; Smirnova, Z. S.; Severin, S. E.; Uhl, R.; Kock, M.; Geiger, K. D.; Gelperina, S. E. Chemotherapy of Glioblastoma in Rats Using Doxorubicin-loaded Nanoparticles. *Int. J. Cancer* **2004**, *109*, 759−767.

(13) Dreher, M. R.; Liu, W.; Michelich, C. R.; Dewhirst, M. W.; Yuan, F.; Chilkoti, A. Tumor Vascular Permeability, Accumulation, and Penetration of Macromolecular Drug Carriers. *J. Natl. Cancer Inst.* **2006**, *98*, 335−344.

(14) Champion, J. A.; Katare, Y. K.; Mitragotri, S. Particle Shape: A New Design Parameter for Micro- and Nanoscale Drug Delivery Carriers. *J. Controlled Release* **2007**, *121*, 3−9.

(15) May, R. C.; Machesky, L. M. Phagocytosis and Actin Cytoskeleton. *J. Cell. Sci.* **2001**, *114*, 1061−1077.

(16) Rejman, J.; Oberle, V.; Zuhorn, I. S.; Hoekstra, D. Size-dependent Internalization of Particles Via the Pathways of Clathrin- and Caveolae-mediated Endocytosis. *Biochem. J.* **2004**, *377*, 159−169.

(17) Qi, X.; Maitani, Y.; Nagai, T.; Wei, S. Comparative Pharmacokinetics and Antitumor Efficacy of Doxorubicin Encapsulated in Soybean-derived Sterols and Poly(ethylene glycol) Liposomes in Mice. *Int. J. Pharm.* **1997**, *146*, 31−39.

(18) Chithrani, B. D.; Chan, W. C. W. Elucidating the Mechanism of Cellular Uptake and Removal of Protein-coated Gold Nanoparticles of Different Sizes and Shapes. *Nano Lett.* **2007**, *7*, 1542−50.

(19) Chithrani, B. D.; Ghazani, A. A.; Chan, W. C. W. Determining the Size and Shape Dependence of Gold Nanoparticle Uptake into Mammalian Cells. *Nano Lett.* **2006**, *6*, 662−668.

(20) Ciofani, G.; Danti, S.; Genchi, G. G.; Mazzolai, B.; Mattoli, V. Boron Nitride Nanotubes: Biocompatibility and Potential Spill-over in Medicine. *Small* **2013**, *9*, 1672−1685.

(21) Chen, X.; Wu, P.; Rousseas, M.; Okawa, D.; Gartner, Z.; Zettl, A.; Bertozzi, C. R. Boron Nitride Nanotubes Are Noncytotoxic and Can be Functionalized for Interaction with Proteins and Cells. *J. Am. Chem. Soc.* **2009**, *131*, 890−891.

(22) Horváth, L.; Magrez, A.; Golberg, D.; Zhi, C. Y.; Bando, Y.; Smajda, R.; Horváth, E.; Forró, L.; Schwaller, B. *In Vitro* Investigation of the Cellular Toxicity of Boron Nitride Nanotubes. *ACS Nano* **2011**, *5*, 3800−3810.

(23) Ciofani, G.; Del Turco, S.; Rocca, A.; de Vito, G.; Cappello, V.; Yamaguchi, M.; Li, X.; Mazzolai, B.; Basta, G.; Gemmi, M.; Piazza, V.; Golberg, D.; Mattoli, V. Cytocompatibility Evaluation of Gum Arabic-coated Ultra-pure Boron Nitride Nanotubes on Human Cells. *Nanomedicine* **2014**, *9*, 773−788.

(24) Li, X.; Zhi, C.; Hanagata, N.; Yamaguchi, M.; Bando, Y.; Golberg, D. Boron Nitride Nanotubes Functionalized with Mesoporous Silica for Intracellular Delivery of Chemotherapy Drugs. *Chem. Commun.* **2013**, *49*, 7337−7339.

(25) Li, X.; Hanagata, N.; Wang, X.; Yamaguchi, M.; Yi, W.; Bando, Y.; Golberg, D. Multimodal Luminescent-magnetic Boron Nitride Nanotubes@NaGdF4:Eu Structures for Cancer Therapy. *Chem. Commun.* **2014**, *50*, 4371−4374.

DOI: 10.1021/acsami.5b04101
ACS Appl. Mater. Interfaces 2015, 7, 17217−17225

(26) Tang, C.; Bando, Y.; Sato, T.; Kurashima, K. A Novel Precursor for Synthesis of Pure Boron Nitride Nanotubes. *Chem. Commun.* **2002**, *12*, 1290−1291.
(27) Terrones, M.; Charlier, J. C.; Gloter, A.; Cruz-Silva, E.; Terrés, E.; Li, Y. B.; Vinu, A.; Zanolli, Z.; Dominguez, J. M.; Terrones, H.; Bando, Y.; Golberg, D. Experimental and Theoretical Studies Suggesting the Possibility of Metallic Boron Nitride Edges in Porous Nanourchins. *Nano Lett.* **2008**, *8*, 1026−1032.
(28) Moon, O. M.; Kang, B. C.; Lee, S. B.; Boo, J. H. Temperature Effect on Structural Properties of Boron Oxide Thin Films Deposited by MOCVD Method. *Thin Solid Films* **2004**, *464*−*465*, 164−169.
(29) Ying, Z. F.; Yu, D.; Ling, H.; Xu, N.; Lu, Y. F.; Sun, J.; Wu, J. D. Synthesis of BCN Thin Films by Nitrogen Ion Beam Assisted Pulsed Laser Deposition From a B_4C Target. *Diamond Relat. Mater.* **2007**, *16*, 1579−1585.
(30) Ciofani, G.; Danti, S.; D'Alessandro, D.; Moscato, S.; Menciassi, A. Assessing Cytotoxicity of Boron Nitride Nanotubes: Interference with the MTT Assay. *Biochem. Biophys. Res. Commun.* **2010**, *394*, 405−411.
(31) Belyanskaya, L.; Manser, P.; Spohn, P.; Bruinink, A.; Wick, P. The Reliability and Limits of the MTT Reduction Assay for Carbon Nanotubes-cell Interaction. *Carbon* **2007**, *45*, 2643−2648.
(32) Macia, E.; Ehrlich, M.; Massol, R.; Boucrot, E.; Brunner, C.; Kirchhausen, T. Dynasore, a Cell-permeable Inhibitor of Dynamin. *Dev. Cell* **2006**, *10*, 839−850.
(33) Fletcher, J. I.; Haber, M.; Henderson, M. J.; Norris, M. D. ABC Transporters in Cancer: More than Just Drug Efflux Pumps. *Nat. Rev. Cancer* **2010**, *10*, 147−156.
(34) Kirtane, A.; Kalscheuer, S.; Panyam, J. Exploiting Nanotechnology to Overcome Tumor Drug Resistance: Challenges and Opportunities. *Adv. Drug Delivery Rev.* **2013**, *65*, 1731−1747.
(35) Lengyel, E. Ovarian Cancer Development and Metastasis. *Am. J. Pathol.* **2010**, *177*, 1053−1064.
(36) Hao, H.; Ma, Q.; He, F.; Yao, P. Doxorubicin and Fe_3O_4 Loaded Albumin Nanoparticles with Folic Acid Modified Dextran Surface for Tumor Diagnosis and Therapy. *J. Mater. Chem. B* **2014**, *2*, 7978−7987.
(37) Wu, J.; Wang, Y.; Jiang, W.; Xu, S.; Tian, R. Synthesis and Characterization of Recyclable Clusters of Magnetic Nanoparticles as Doxorubicin Carriers for Cancer Therapy. *Appl. Surf. Sci.* **2014**, *321*, 43−9.
(38) Regli, S.; Kelly, J. A.; Barnes, M. A.; Andrei, C. M.; Veinot, J. G. C. Mesoporous Silica Encapsulation of Silicon Nanocrystals: Synthesis, Aqueous Dispersibility and Drug Release. *Mater. Lett.* **2014**, *115*, 21−24.
(39) Vimala, K.; Sundarraj, S.; Paulpandi, M.; Vengatesan, S.; Kannan, S. Green Synthesized Doxorubicin Loaded Zinc Oxide Nanoparticles Regulates the Bax and Bcl-2 Expression in Breast and Colon Carcinoma. *Process Biochem.* **2014**, *49*, 160−172.
(40) Nigam, S.; Chandra, S.; Newgreen, D. F.; Bahadur, D.; Chen, Q. Poly(ethylene glycol)-modified PAMAM-Fe_3O_4-doxorubicin Triads with the Potential for Improved Therapeutic Efficacy: Generation-dependent Increased Drug Loading and Retention at Neutral pH and Increased Release at Acidic pH. *Langmuir* **2014**, *30*, 1004−1011.
(41) Murali, R.; Vidhya, P.; Thanikaivelan, P. Thermoresponsive Magnetic Nanoparticle - Aminated Guar Gum Hydrogel System for Sustained Release of Doxorubicin Hydrochloride. *Carbohydr. Polym.* **2014**, *110*, 440−445.
(42) Gillies, E. R.; Fréchet, J. M. pH-Responsive Copolymer Assemblies for Controlled Release of Doxorubicin. *Bioconjugate Chem.* **2005**, *16*, 361−368.
(43) Che, E.; Wan, L.; Zhang, Y.; Zhao, Q.; Han, X.; Li, J.; Liu, J.; Wang, J. Development of Phosphonate-terminated Magnetic Mesoporous Silica Nanoparticles for pH-controlled Release of Doxorubicin and Improved Tumor Accumulation. *Asian J. Pharm. Sci.* **2014**, *9*, 317.
(44) Yang, C. K. Exploring the Interaction Between the Boron Nitride Nanotube and Biological Molecules. *Comput. Phys. Commun.* **2011**, *182*, 39−42.
(45) Mukhopadhyay, S.; Gowtham, S.; Scheicher, R. H.; Pandey, R.; Karna, S. P. Theoretical Study of Physisorption of Nucleobases on Boron Nitride Nanotubes: a New Class of Hybrid Nano-biomaterials. *Nanotechnology* **2010**, *21*, 165703−165709.
(46) Moradi, A. V.; Peyghan, A. A.; Hashemian, S.; Baei, M. T. Theoretical Study of Thiazole Adsorption on the (6,0) zigzag Single-Walled Boron Nitride Nanotube Bull. *Bull. Korean Chem. Soc.* **2012**, *33*, 3285−3292.
(47) André, C.; Guillaume, Y. C. Boron Nitride Nanotubes and Their Functionalization via Quinuclidine-3-thiol with Gold Nanoparticles for the Development and Enhancement of the HPLC Performance of HPLC Monolithic Columns. *Talanta* **2012**, *93*, 274−278.
(48) Ciofani, G.; del Turco, S. T.; Genchi, G. G.; D'Alessandro, D.; Basta, G.; Mattoli, V. Transferrin-conjugated Boron Nitride Nanotubes: Protein Grafting, Characterization, and Interaction with Human Endothelial Cells. *Int. J. Pharm.* **2012**, *436*, 444−453.
(49) Ferreira, T. H.; Marino, A.; Rocca, A.; Liakos, I.; Nitti, S.; Athanassiou, A.; Mattoli, V.; Mazzolai, B.; de Sousa, E. M. B.; Ciofani, G. Folate-grafted Boron Nitride Nanotubes: Possible Exploitation in Cancer Therapy. *Int. J. Pharm.* **2015**, *481*, 56−63.
(50) Menichetti, L.; De Marchi, D.; Calucci, L.; Ciofani, G.; Menciassi, A.; Forte, C. Boron Nitride Nanotubes for Boron Neutron Capture Therapy as Contrast Agents in Magnetic Resonance Imaging at 3 T. *Appl. Radiat. Isot.* **2011**, *69*, 1725−1727.
(51) Iizumi, Y.; Okazaki, T.; Zhang, M.; Yuge, R.; Ichihashi, T.; Nakamura, M.; Ikehara, Y.; Iijima, S.; Yudasaka, M. Preparation and Functionalization of Boron Nitride Containing Carbon Nanohorns for Boron Neutron Capture Therapy. *Carbon* **2015**, *93*, 595−603.
(52) Yamakov, V.; Park, C.; Kang, J. H.; Wise, K. E.; Fay, C. Piezoelectric Molecular Dynamics Model for Boron Nitride Nanotubes. *Comput. Mater. Sci.* **2014**, *95*, 362−370.
(53) Zhong, B.; Tang, X. H.; Huang, X. X.; Xia, L.; Zhang, X. D.; Wang, C. J.; Wen, G. W. Boron Nitride Hollow Nanospheres: Synthesis, Formation Mechanism and Dielectric Property. *Mater. Res. Bull.* **2015**, *64*, 61−67.
(54) Ciofani, G.; Raffa, V.; Menciassi, A.; Cuschieri, A. Boron Nitride Nanotubes: An Innovative Tool for Nanomedicine. *Nano Today* **2009**, *4*, 8−10.

DOI: 10.1021/acsami.5b04101
ACS Appl. Mater. Interfaces 2015, 7, 17217−17225